JME

Journal of Mining & Environment,
Vol. 9, No. 4, 2018, 893-904.
DOI: 10.22044/jme.2018.6129.1428

Behavior of a hydraulic fracture in permeable formations

A. Abdollahipour[1*], M. Fatehi-Marji[2], H. Soltanian[1], E.A. Kazemzadeh[1]

1. Division of Petroleum Engineering, Faculty of upstream Petroleum Industry, Research Institute of Petroleum Industry (RIPI), Tehran, Iran
2. Department of Mining and Metallurgical Engineering, Yazd University, Yazd, Iran

Received 16 August 2017; received in revised form 22 May 2018; accepted 9 June 2018
**Corresponding author: abdollahipoura@ripi.ir (A. Abdollahipour).*

Abstract
The permeability and coupled behavior of pore pressure and deformations play an important role in hydraulic fracturing (HF) modeling. In this work, a poroelastic displacement discontinuity method is used to study the permeability effect on the HF development in various formation permeabilities. The numerical method is verified by the existing analytical and experimental data. Then the propagation of a hydraulic fracture in a formation with a range of permeabilities is studied. The time required for propagation of an HF to 10 times its initial length is used to compare the propagation velocity in the formations with different permeabilities. The results obtained show that the HF propagation can be significantly delayed by a permeability less than almost 10^{-9} D. Also the effect of HF spacing on the propagation path is studied. It was shown that the stress shadowing effect of HFs remained for a longer spacing than in the elastic model due to the required time for fluid leak-off in the formation. Also the propagation angles are higher in the poroelastic model predictions than the elastic model. Therefore, it is proposed to use the poroelastic model when studying multi-HF propagation in order to avoid errors caused by neglecting the pore fluid effects on the HF propagation paths.

Keywords: *Hydraulic Fracture, Poroelastic Formations, Permeability, Crack Propagation.*

1. Introduction

Hydraulic fracturing (HF) is among the most popular methods used in the oil and gas exploitation industry to increase the production rate. HF improves the natural connection of the wellbore and the reservoir by creating new fractures. Although this method is widely used in industry, there are yet some aspects that require further investigations to eventually lead to a better understanding of the mechanism of this method. Normally, rocks contain discontinuities (such as fractures and faults) and pore fluids. The presence of pore fluids in these discontinuities can significantly affect the stress and displacement fields of a rock mass. It has been shown that the crack propagation path may be different in a porous medium due to changes in the fluid flow and pore pressure [1]. The effect of permeability and porosity of a formation on the propagation of a hydraulic fracture and its pattern requires further investigations. In most studies, an elastic isotropic medium is considered for crack propagation [2-6], while HF is mostly used in formations with a very low permeability (i.e. shale formations). The initial permeability of the formation may substantially affect the propagation of a pressurized crack (i.e. hydraulic fracture).

In many geomechanics problems such as hydraulic fracturing [7-9], the in-situ stress measurement [10-12], geothermal energy extraction process [13-16], and pore fluid and its subsequent effects play a crucial role. There have been a number of studies on the derivation of analytical or numerical solutions for the hydraulic fracturing problem in a poroelastic medium [9, 17-20]. Ghasemi et al. have combined the displacement discontinuity and finite element methods to solve the problem of fracture flow and rock deformation in a hydraulic fracture simulation [21]. Huang and Ghasemi have studied the evolution of fractured reservoirs during gas production [22]. Combining the finite element/boundary element methods, Safari and Ghasemi have investigated the effect of injection on the hydraulic fracture/natural fracture [23]. However, the propagation of a hydraulic fracture in a poroelastic medium has rarely been studied. Abhishek et al. have studied crack propagation in a pre-stressed inhomogeneous medium influenced by shear wave [24]. Remij et al. have studied the mode-II fracture propagation in a poroelastic medium using XFEM [25]. Abdollahipour et al. have developed a poroelastic displacement discontinuity method and investigated the propagation of a crack in a porous medium in various time intervals [9, 26]. Zhou et al. have determined the crack propagation angle of a hydraulic fracture under hydrodynamic and hydrostatic pressure joint action [27]. Ren et al. have studied hydraulic fracture propagation in two adjacent horizontal wells in an ultra-low permeability formation [28].

Fluid pressure change induces a change in the matrix deformation and stresses, and at the same time, matrix deformation induces a change in the fluid volume and fluid pressure. These pore pressure and stress changes affect the fracture, and incur further fracture deformation. Biot [29-31] has pioneered the poroelastic theory, which accounts for these coupled interactions. The fundamental solution to the displacement discontinuity method (DDM) contains a displacement jump. Therefore, this method is ideal for problems involving fractures and discontinuities. However, the original formulation of DDM [32] and its higher order implementations [33-35, 1, 36, 37] are limited to the elastic problems. In the poroelastic studies of fractures, DDM has been previously coupled with other numerical methods such as FDM and FEM [38-40].

In this work, a fully coupled hydro-mechanical DDM model is used to investigate numerically the effect of initial permeability of the formation on the propagation of hydraulically induced fractures. First, the formulation is briefly introduced, and then after verification of the proposed method, a variety of numerical models are build and analyzed to investigate the effect of permeability and fracture spacing on fracture propagation.

2. Research methodology

A constant element poroelastic-displacement discontinuity method (CEP-DDM) [1, 9, 26] will be used to account for the coupling effects of pore pressure and matrix deformation.

The effect of permeability change allowing a pore fluid flow has been considered in the analyses. The pore pressure is distributed uniformly in the fractures. Table 1 shows the hydro-mechanical (based on field data) properties used in the modelings [41-45]. The following assumptions and simplifications are used in the analyses:

- σ_x = 57 MPa and σ_y = 47 MPa are two far-field orthogonal stresses acting in a plane.
- Crack propagation angle in models is predicted based on the σ fracture criterion proposed by Erdogan and Sih [46].
- The propagation of cracks in the CEP-DDM model is based upon the algorithm shown in Figure 1.

Table 1. Hydro-mechanical properties of rocks used in analyses [41-45].

Rock	G	K	ν	K_u	ν_u	K_m	α	B	M	ϕ	k	c
Ruhr sandstone	9	13	0.12	30	0.31	36	0.65	0.88	41	0.02	0.20	5.3×10^{-3}
Tennessee Granite	24	40	0.25	44	0.27	50	0.19	0.51	81	0.02	0.0001	1.3×10^{-5}
Granite	19	35	0.27	41	0.30	45	0.27	0.55	84	0.02	0.0001	7×10^{-6}
Berea Sandstone	6	8	0.20	16	0.33	36	0.79	0.62	12	0.19	190	6
Westerly Granite	15	25	0.25	42	0.34	45	0.47	0.85	75	0.01	0.0004	2.2×10^{-5}
Weber Sandstone	12	13	0.15	25	0.29	36	0.64	0.73	0.28	0.06	1	2.1×10^{-2}
Ohio Sandstone	6.8	8.4	0.18	13	0.28	39	0.74	0.50	9	0.19	5.6	3.9×10^{-2}
Pecos Sandstone	5.9	6.7	0.16	14	0.31	41	0.83	0.61	10	0.20	0.8	5.4×10^{-3}
Boise Sandstone	4.2	4.6	0.15	8.3	0.31	42	0.85	0.50	4.7	0.26	800	4×10^{-1}

where G, K, and ν are the shear modulus, bulk modulus, and Poisson's ratio, respectively. The subscript u presents the undrained parameters, α is the Biot coefficient, B is the Skempton's coefficient, M is the Biot modulus, Φ is the porosity, k is the permeability, and c is the generalized consolidation coefficient.

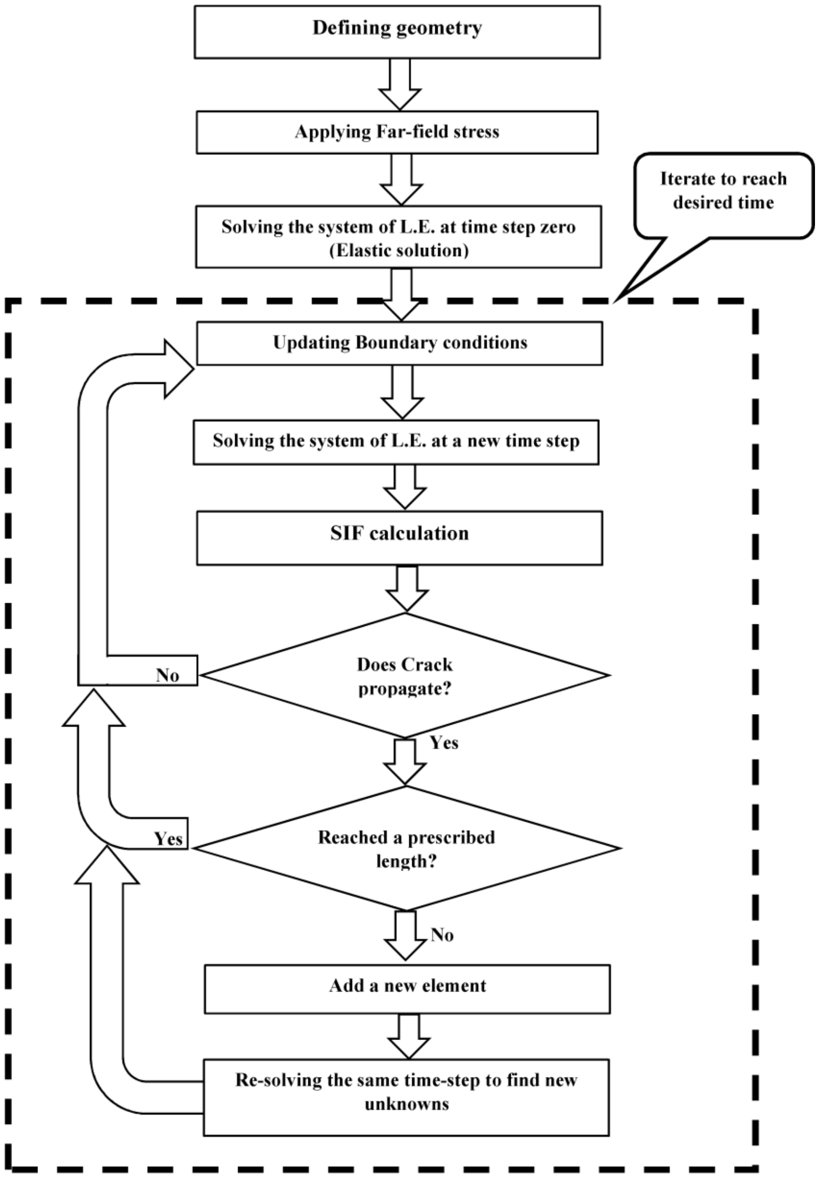

Figure 1. Algorithm used in CEP-DDM for crack propagation in a poroelastic medium [9].

3. Constant element poroelastic DDM

Originally, DDM was proposed and formulated for the analysis of elastic media. Its inherent formulation based on a displacement jump made this boundary element method ideal for the study of fracture mechanics problems. However, DDM can only model fractures according to the elasticity theory. Pore pressure and its coupling effect with mechanical deformation play an important role in many geomechanics problems such as hydraulic fracturing. To consider these effects in DDM, it should be extended to the poroelasticity theory, which accounts for the hydro-mechanical effects of a porous environment. DDM requires a fundamental poroelastic solution for an extension to poroelasticity. Based on the dislocation theory, Abdollahipour derived a point-plane strain displacement discontinuity solution in a poroelastic medium [1]. Appendix A presents this solution.

The influence functions of a poroelastic-based DDM may be found by distributing the solution presented in appendix A over a domain of Ψ^{Γ} in the direction of s axis in Figure 2. Consider local stress in the direction of s axis in Figure 2 due to a unit normal displacement discontinuity ($D_n = 1$). It can be obtained using the following integrals.

$$\left(\sigma_{xx}^{dn}\right)^0 = \int_{-a}^{a} \left(\sigma_{112}\right)^0 d\lambda \tag{1}$$

$$\Delta\left(\sigma_{xx}^{ds}\right) = \int_{-a}^{a} \Delta\sigma_{112} d\lambda \tag{2}$$

where $(\sigma_{112})^0$ and $\Delta\sigma_{112}$ are the fundamental solutions presented in Eqs. (A.3) and (A.4), considering i = j = 1 and k = 2. The complete

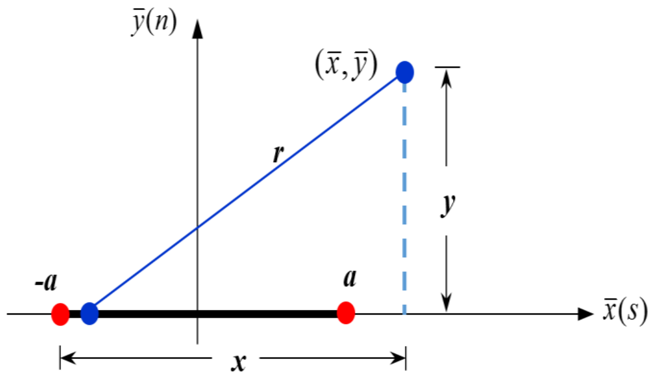

Figure 2. An element in local coordinates.

influence functions (including a time-independent part and a time-dependent part) have been described by Abdollahipour et al. [20, 9].

The original DDM contains two discontinuities, i.e. normal and shear displacement discontinuities (D_s and D_n, respectively). Poroelastic DDM adds one more discontinuity for flux D_f. These three discontinuities are unknown at the beginning of the numerical simulations in many fracture problems in poroelastic formations. Rather they must be solved incrementally in the time domain, while considering stress and pore pressure histories for each element. Hence, histories of pore pressures and stresses are used to build a set of equations to be used in the numerical implementation of the method [9].

A set of three integral equations (one integral equation for each discontinuity) can be used to determine the displacement and flux discontinuities. As shown in Eqs. (3)-(5), these integrals are based upon the displacement and flux discontinuity histories of shear stress, normal stress, and pore pressure.

$$\begin{aligned}\sigma_s(x,t) = l_{i2}(x) l_{j1}(x) \Big[&\int_0^t \int_\Psi l_{ik}(\lambda) l_{jl}(\lambda) \sigma_{kl}^{ds}(x,\lambda,t-\Omega) D_s(\lambda,\Omega) d\Psi(\lambda) d\Omega \\ &+ \int_0^t \int_\Psi l_{ik}(\lambda) l_{jl}(\lambda) \sigma_{kl}^{dn}(x,\lambda,t-\Omega) D_n(\lambda,\Omega) d\Psi(\lambda) d\Omega \\ &+ \int_0^t \int_\Psi l_{ik}(\lambda) l_{jl}(\lambda) \sigma_{kl}^{df}(x,\lambda,t-\Omega) D_f(\lambda,\Omega) d\Psi(\lambda) d\Omega \Big]\end{aligned} \tag{3}$$

$$\begin{aligned}\sigma_n(x,t) = l_{i2}(x) l_{j2}(x) \Big[&\int_0^t \int_\Psi l_{ik}(\lambda) l_{jl}(\lambda) \sigma_{kl}^{ds}(x,\lambda,t-\Omega) D_s(\lambda,\Omega) d\Psi(\lambda) d\Omega \\ &+ \int_0^t \int_\Psi l_{ik}(\lambda) l_{jl}(\lambda) \sigma_{kl}^{dn}(x,\lambda,t-\Omega) D_n(\lambda,\Omega) d\Psi(\lambda) d\Omega \\ &+ \int_0^t \int_\Psi l_{ik}(\lambda) l_{jl}(\lambda) \sigma_{kl}^{df}(x,\lambda,t-\Omega) D_f(\lambda,\Omega) d\Psi(\lambda) d\Omega \Big]\end{aligned} \tag{4}$$

$$\begin{aligned}p(x,t) = &\int_0^t \int_\Psi P_s(x,\lambda,t-\Omega) D_s(\lambda,\Omega) d\Psi(\lambda) d\Omega \\ &+ \int_0^t \int_\Psi P_n(x,\lambda,t-\Omega) D_n(\lambda,\Omega) d\Psi(\lambda) d\Omega \\ &+ \int_0^t \int_\Psi P_f(x,\lambda,t-\Omega) D_f(\lambda,\Omega) d\Psi(\lambda) d\Omega\end{aligned} \tag{5}$$

where Ψ is the element locus, and i, j, k, and l are subscripts that vary from 1 to 2 assuming the Einstein's summation convention on them. In Figure 3, (x,y) is the global coordinate system and $(\bar{x}_1, \bar{x}_2)$ is the local coordinate system whose axes, $\bar{x}_1$ and $\bar{x}_2$, respectively, coincide with the tangential (s) and normal (n) directions of the element.

The influence function ($\sigma_{kl}^{dn}(x,\lambda,t-\Omega)$) is a local stress component at point x and time t due to a unit normal displacement discontinuity located at λ and occurring at time Ω. Other functions (σ_{kl}^{ds} and σ_{kl}^{df}) have similar meanings. P_s, P_n, and P_f are the influence functions for shear and normal displacement discontinuities and flux discontinuities D_s, D_n, and D_f, respectively.

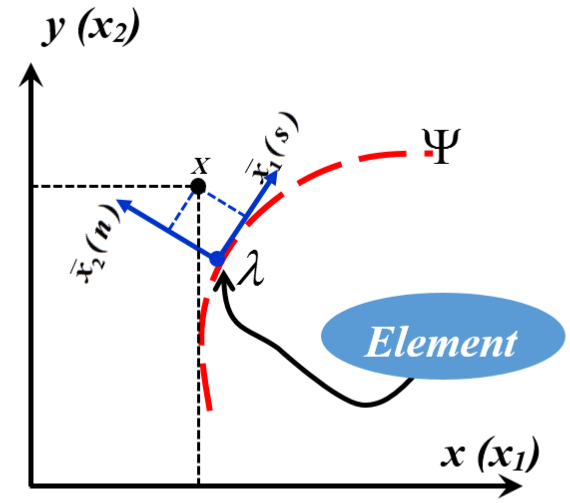

Figure 3. Global and local coordinate systems.

Considering constant elements and using collocation points at the mid-point of each element, the discontinuities are distributed constantly over each element. Constant time steps Δt are considered, and D_s, D_n, and D_f change linearly with time.

The system of Eqs. (3)-(5) is numerically solved according to the following steps:

- Discretization of the geometry into m elements.
- Discretization of the time to h steps from 0 to t.
- Approximation of D_s, D_n, and D_f over each element $\Gamma \in [1, m]$ and time-step $\omega \in [1, h]$.
- Construction of a linear system of equations based on the numerical integration of Eqs. (3)- (5).
- Solving the system of equations at the end of the first Δt, and determination of D_s, D_n, and D_f at the middle of each element.
- D_s, D_n, and D_f are marched through time, at the end of each, Δt is found until reaching the last Δt.

Following the above steps, Eqs. (3)-(5) may be presented in a double-summation form of integrals over time and space. For example, Eq. (4) at point x^α and time t may be presented as:

$$\begin{aligned}\sigma_n^h(x^\alpha, t) = l_{i2}^\alpha l_{j1}^\alpha \sum_{\omega=1}^{h} \sum_{\Gamma=1}^{m} l_{ik}^\Gamma l_{jl}^\Gamma \times \\ \Big\{ \int_0^{\Delta t} \Big[D_n^\Gamma((\omega-1)\Delta t + \Omega) \int_{\Psi^\Gamma} \sigma_{kl}^{dn}(x^\alpha, \lambda, (h-\omega+1)\Delta t - \Omega) d\Psi(\lambda) \Big] d\Omega + \\ \int_0^{\Delta t} \Big[D_s^\Gamma((\omega-1)\Delta t + \Omega) \int_{\Psi^\Gamma} \sigma_{kl}^{ds}(x^\alpha, \lambda, (h-\omega+1)\Delta t - \Omega) d\Psi(\lambda) \Big] d\Omega + \\ \int_0^{\Delta t} \Big[D_f^\Gamma((\omega-1)\Delta t + \Omega) \int_{\Psi^\Gamma} \sigma_{kl}^{df}(x^\alpha, \lambda, (h-\omega+1)\Delta t - \Omega) d\Psi(\lambda) \Big] d\Omega \Big\}\end{aligned} \tag{6}$$

The discretization of 3 parts of Eq. (6) are collocated at the middle of all elements for normal stress boundary condition σ_n. Following a similar procedure, the coefficients σ_s and p can be obtained. Eventually, for a total of M boundary elements, there will be 3M linear equations for 3M unknown discontinuities (D_n, D_s, D_f) at any time t. These linear equations can be presented by matrix notation as:

$$AD^h = \sigma^h - \sum_{\omega=0}^{h-1} B^n D^n \tag{7}$$

The complete procedure and formulation have been explained in our previously published work [20]. We further implemented an algorithm to simulate crack propagation in a porous rock [9]. A combination of these methods will be used in the following sections to study the effect of permeability on HF propagation.

4. Verification of proposed method

The constant element poroelastic-displacement discontinuity method (CEP-DDM) is evaluated against an analytical solution as well as the field measurement results.

4.1. A suddenly pressurized crack

Sneddon has provided the exact crack opening displacement for a pressurized crack based on the elasticity theory. The crack has a length of 2L (with $-L \le x \le L$, i.e. the crack center coincides with the origin of the coordinate system) and is pressurized by internal pressure p, as shown in Figure 4 [47].

$$w_f = \frac{2p(1-\nu)}{G}\sqrt{L^2 - x^2} \tag{8}$$

where p is the internal pressure, G is the shear modulus, ν is the Poisson's ratio, L is the crack half-length, and x is the distance from the crack center.

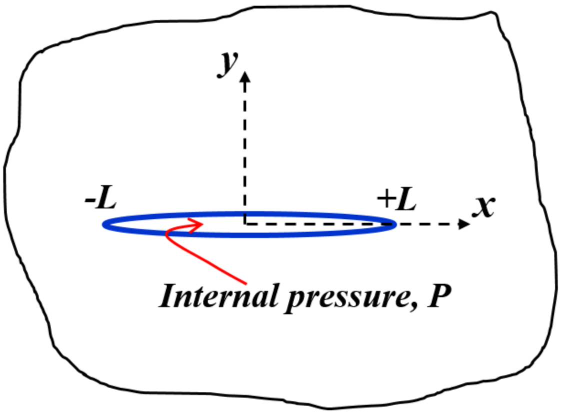

Figure 4. Pressurized crack of Sneddon's problem.

A poroelastic medium exhibits two distinct behaviors. At the very beginning of the loading, the pore fluid cannot dissipate. Therefore, the poroelastic medium shows an elastic response with undrained parameters. As time passes by, the pore pressure migrates to further boundaries, and eventually dissipates completely. At this time, a drained behavior (i.e. elastic response of the medium with drained parameters) emerges. Hence, the Sneddon's solution may be used to predict the early and late behaviors of the crack opening displacement in a poroelastic rock simply by using the undrained and drained parameters, respectively. The numerical results for crack opening at the first time step is compared with the Sneddon's solution using the undrained parameters, while the numerical results at t = 8000 s are compared with the results of the Sneddon's solution using the drained parameters. A length of L = 0.5 m and the properties of Table 2 with an internal pressure of 30 MPa and a time step size of $\Delta t = 0.05$ s are used for verification. Parameter B in Table 2 is the Skempton's coefficient. Figure 5 presents the numerical and analytical results for a pressurized crack.

As it can be seen, the numerical results (using only 20 constant elements in the numerical model) match the analytical results well in both the drained and undrained conditions.

Table 2. Rock properties for suddenly pressurized crack verification.

Parameter	Value
G(GPa)	13
ν_u	0.31
ν	0.12
k(mdarcy)	1
φ	0.02
α	0.65
c (m^2/s)	0.002
B	0.88

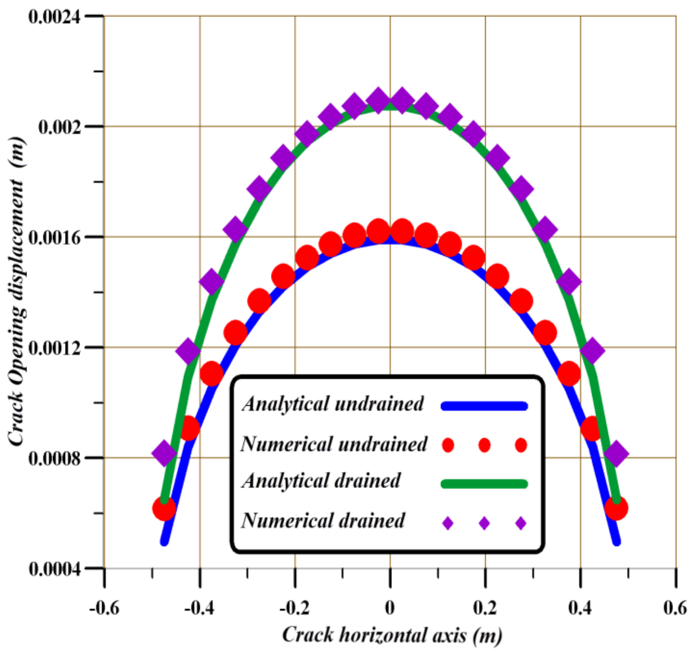

Figure 5. Analytical and numerical results of the crack opening displacement in a short time (undrained condition) and a long time (drained condition) after loading initiation.

4.2. Field measurements

Rito and Emura [48] have measured time changes of the pore water pressure in a 400 m drilled borehole. A mud weight pressure of 2960 KPa was reported for the bottom of the borehole. They measured the pore pressure by a GD-CONE measurement equipment at a 60 cm distance from the bottom hole. Figure 6 shows a scheme of the borehole and measurement location. Figure 7 demonstrates the numerical and field measurement results of pore pressure changes. The pore pressure was measured for 20000 s in the field; however, since the numerical results reached a constant pressure, these results are only provided for 14000 s. The pore pressure predicted by the numerical model converges the mud weight pressure (2960 KPa), as expected. However, the field measurements are slightly lower (almost 2800 KPa) at the end of the measurements. It can be due to the lost circulation effects neglected in numerical simulation. The ability of the numerical model in prediction of the time-dependent behavior is well-presented in both verification examples. This verifies the accuracy and applicability of the proposed numerical model.

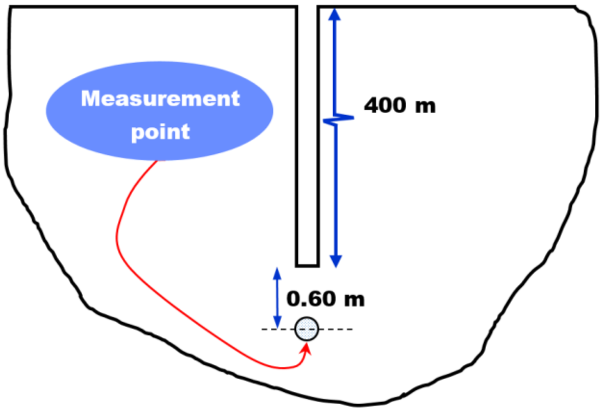

Figure 6. Field measurement of pore pressure at 400 m depth.

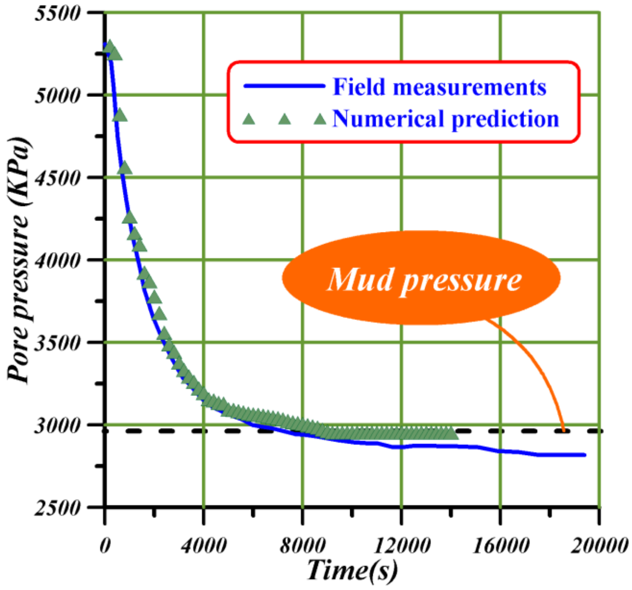

Figure 7. Numerical and field measurement results of changes of pore pressure with time.

5. Effect of permeability on hydraulic fracture propagation

In order to investigate the effect of permeability on the crack propagation time, a hydraulic fracture in a poroelastic medium was considered. The required time for a crack to propagate to 10 times its original length was recorded in numerical modeling. Various permeabilities for reservoir rocks from 1 mD to 1 pD (based on Table 1), which is equivalent to high permeable rocks such as sandstones to very low permeable rocks such as shales, were considered in numerical models. A crack of length 50 cm was used in the initial model. Time steps for the time-dependent analyses were constant and equal to $\Delta t = 0.05$ s.

As illustrated in Figure 8, reduction of permeability has resulted in an increase in the propagation time or, in other words, slower HF propagation. However, a significant change in the propagation time or speed appears in the substantial changes of permeability. The most required time for HF propagation is for very low permeable rocks, i.e. shales and tight gas formations. Fluids in a rock with a lower permeability require a longer time to migrate from a crack to the reservoir; hence, reducing the HF propagation speed. Since the hydraulic fracture length in a low permeability formation is the key to a successful HF operation, the results of these modelings show the requirement of a higher pumping time for a hydraulic fracturing of these reservoirs.

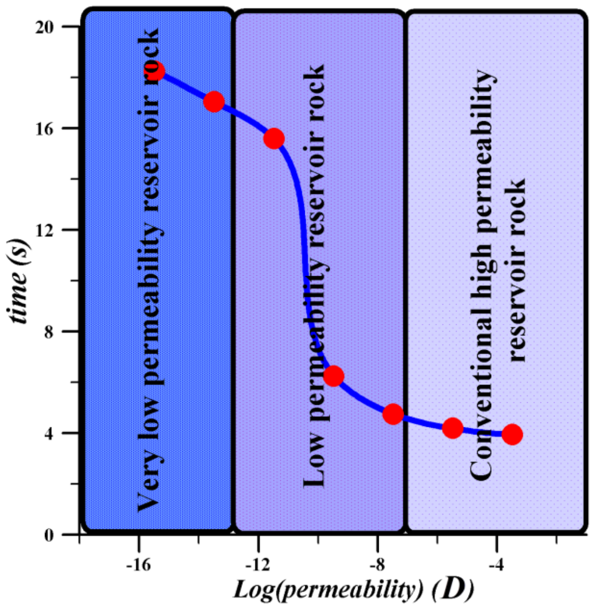

Figure 8. Required time for a crack propagation to 10 times its initial length in rocks with various permeabilities.

6. Effect of spacing on initial HF propagation angle

Neighboring HFs may affect the initial propagation path of each other. In order to investigate this effect, 2 HFs with various spacings were considered. The same loading conditions as the previous models were used. The numerical study was carried out considering the elastic and poroelastic conditions to simultaneously compare the effect of permeability and hydro-mechanical coupling on the propagation paths. Initial HFs have initial lengths of L = 1 m. A ratio of spacing to initial HF length of S/L = 0.25, 0.5, 0.75, 1.0, 1.5, 2.0, and 4.0 for models and S/L = 0.25, 0.5, 0.75, 1.0, 1.5, 2.0, 6.0, 8.0, and 10.0 were used for the elastic and poroelastic models, respectively. The properties are based on Table 2 for both the elastic and poroelastic models. It is clear in Figures 9 and 10 that in a closer HF spacing, propagations are diverging from the adjacent HF. In the elastic study, the effect of adjacent HF is diminished after S/L = 4.0. However, the situation is quite different in the same model but under poroelastic conditions in Figure 10.

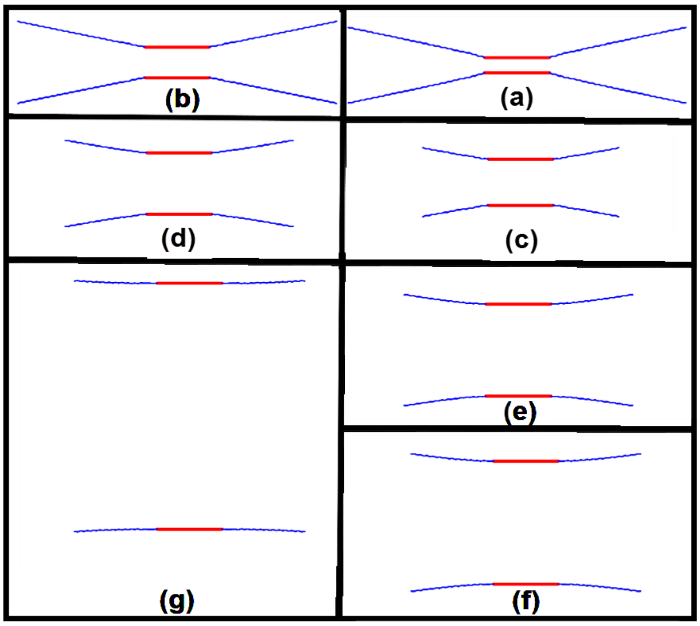

Figure 9. HF propagation of two adjacent cracks in elastic medium. (a) to (g) correspond to S/L = 0.25, 0.5, 0.75, 1.0, 1.5, 2.0, and 4.0.

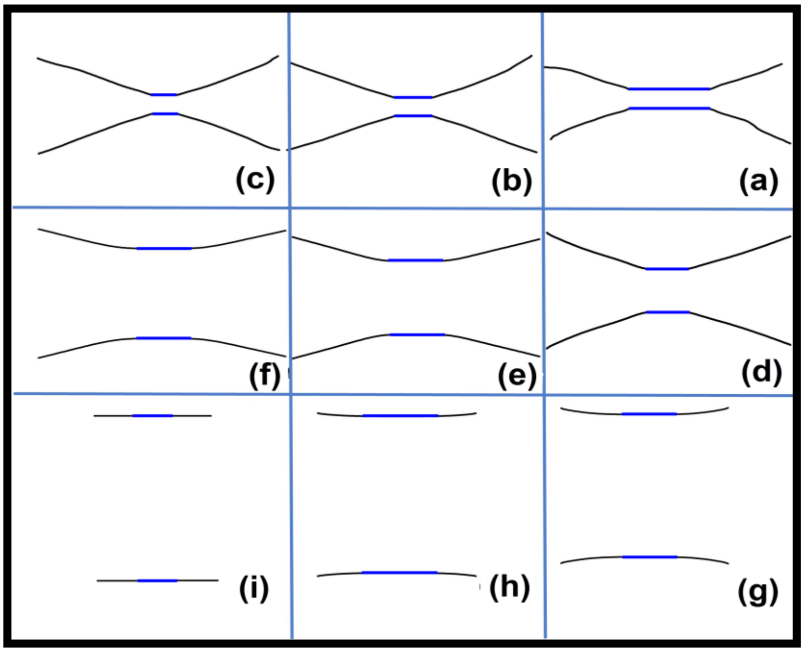

Figure 10. HF propagation of two adjacent cracks in poroelastic medium. (a) to (i) correspond to S/L = 0.25, 0.5, 0.75, 1.0, 1.5, 2.0, 6.0, 8.0, and 10.0.

The adjacent HFs keep affecting each other up to S/L = 10. This shows the different behaviors of an elastic study and a poroelastic study. Since fluid penetration into formation takes time, the stress shadowing effect of HFs has remained for a longer spacing than in the elastic model.

Figure 11 compares the initial propagation angles in various S/L values for both modelings. It is clear that for the same S/L ratio, the poroelastic model predicts a higher propagation angle (i.e. a higher diverging angle from the adjacent crack) than the elastic model. This shows that the poroelastic effects may change the predicted propagation path in the presence of more than one crack. The results of HF propagation from elastic studies in multi-HF propagation should be used with caution.

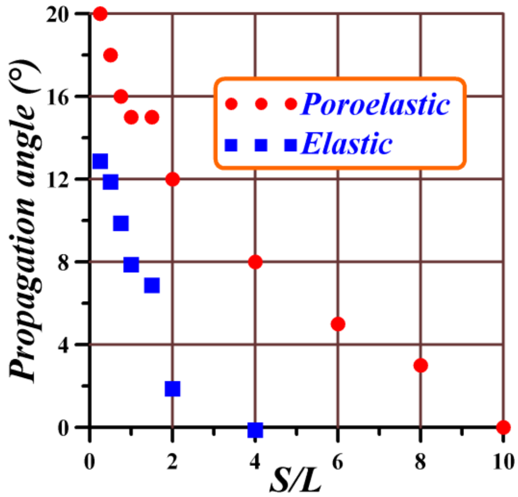

Figure 11. Initial propagation angle for various spacings in elastic and poroelastic analyses of 2 adjacent HFs.

7. Conclusions

The presence of displacement jump in the fundamental solution of DDM makes it ideal for the fracture and discontinuity problems. However, the original formulation of DDM is limited to the elastic problems. Many problems in geomechanics such as geothermal problems and hydraulic fracturing are better presented in a porous medium. A constant element poroelastic displacement discontinuity method (implemented in the CEP-DDM code) was proposed and used to study the effect of permeability on the propagation time of a hydraulically-induced fracture.

Before analyzing the problem, a verification study was performed using an analytical solution and the field measurement results. Both verifications showed a reasonable accuracy and trend of the proposed numerical results with the analytical and field measurement results.

Numerical simulation of the propagation of a hydraulically-induced fracture showed that a decrease in permeability resulted in an increase in the time required for a crack to reach a specified length. It should be noted out that a significant change in the propagation time only appears in the dramatic changes of permeability of the formation. This significant increase of propagation time appears in a permeability less than almost 10^{-9} D, corresponding to low to very low permeability of reservoir rocks.

Also the effect of HF spacing on the propagation path was studied. It was shown that the effect of adjacent HFs on the propagation path in poroelastic models was much more than the elastic models. It was shown that the stress shadowing effect of HFs remained for a longer spacing than in the elastic model because of the required time for fluid leak-off in the formation. It is proposed to use the poroelastic model when studying a multi-HF propagation in order to avoid the errors caused by neglecting the pore fluid effects on the HF propagation paths. Also the propagation angles are different in the elastic and poroelastic models.

References

[1]. Abdollahipour, A. (2015). Crack propagation mechanism in hydraulic fracturing procedure in oil reservoirs. Ph.D Thesis, University of Yazd.

[2]. Abdollahipour, A., Fatehi Marji, M., Yarahmadi-Bafghi, A. and Gholamnejad, J. (2015). Simulating the propagation of hydraulic fractures from a circular wellbore using the Displacement Discontinuity Method. Int J Rock Mech Min Sci. 80: 281-91.

[3]. Kgatle, M.R.R. and Mason, D.P. (2014). Propagation of a linear hydraulic fracture with tortuosity. Int J Non Linear Mech. 61: 39-53.

[4]. Gordeliy, E. and Peirce, A. (2015). Enrichment strategies and convergence properties of the XFEM for hydraulic fracture problems. Comput Methods Appl Mech Eng. 283: 474-502.

[5]. Almi, S., Dal Maso, G. and Toader, R. (2014). Quasi-static crack growth in hydraulic fracture. Nonlinear Anal Theory, Methods Appl. 109: 301-318.

[6]. Lacazette, A. and Geiser, P. (2013). Comment on Davies et al., 2012- Hydraulic fractures: How far can they go?. Marine and Petroleum Geology. 43: 516-518.

[7]. Griffiths, D.V., Huang, J. and Wong, S.W. (2011). In situ stress determination from inversion of hydraulic fracturing data. Int J Rock Mech Min Sci. 48: 476-481.

[8]. Yu, W., Luo, Z., Javadpour, F., Varavei, A. and

Sepehrnoori, K. (2014). Sensitivity analysis of hydraulic fracture geometry in shale gas reservoirs. J Pet Sci Eng. 113: 1-7.

[9]. Abdollahipour, A., Fateh-Marji, M., Yarahmadi-Bafghi, A. and Gholamnejad, J. (2016). Time-dependent crack propagation in a poroelastic medium using a fully coupled hydromechanical displacement discontinuity method. Int J Fract. 199: 71-87.

[10]. Bush, D.D. and Barton, N. (1989). Application of small-scale hydraulic fracturing for stress measurements in bedded salt. Int J Rock Mech Min Sci Geomech Abstr. 26: 629-635.

[11]. Schmitt, D.R. and Zoback, M.D. (1989). Poroelastic effects in the determination of the maximum horizontal principal stress in hydraulic fracturing tests- A proposed breakdown equation employing a modified effective stress relation for tensile failure. Int J Rock Mech Min Sci Geomech Abstr. 26: 499-506.

[12]. Abdollahipour, A., Fatehi Marji, M. and Yarahmadi-Bafghi, A.R. (2013). A fracture mechanics concept of in-situ stress measurement by hydraulic fracturing test. 6th Int. Symp. In-situ Rock Stress, Sendai, Japan: ISRM.

[13]. Reinicke, A. and Zimmermann, G. (2010). Hydraulic stimulation of a deep sandstone reservoir to develop an Enhanced Geothermal System: Laboratory and field experiments. Geothermics. 39: 70-77.

[14]. Legarth, B., Huenges, E. and Zimmermann, G. (2005). Hydraulic fracturing in a sedimentary geothermal reservoir: Results and implications. Int J Rock Mech Min Sci. 42: 1028-1041.

[15]. Hofmann, H., Babadagli, T. and Zimmermann, G. (2014). Hot water generation for oil sands processing from enhanced geothermal systems: Process simulation for different hydraulic fracturing scenarios. Appl Energy. 113: 524-547.

[16]. Davies, R., Foulger, G., Bindley, A. and Styles, P. (2013). Induced seismicity and hydraulic fracturing for the recovery of hydrocarbons. Mar Pet Geol. 45: 171-185.

[17]. Hu, J. and Garagash, D. (2010). Plane-strain propagation of a fluid-driven crack in a permeable rock with fracture toughness. J Engng Mech-ASCE. 136: 1152-1166.

[18]. Greetesma, J. and de Klerk, F. (1969). A rapid method of predicting width and extent of hydraulic induced fractures. J.of Pet Tech. 21: 1571-1581.

[19]. Lobao, M., Eve, R., Owen, D.R.J., de Souza, N.E., Lobão, M.C. and Neto, E.A.D.S. (2010). Modelling of hydro-fracture flow in porous media. Engng Comput. 27:129-154.

[20]. Abdollahipour, A., Fatehi Marji, M., Yarahmadi-Bafghi, A. and Gholamnejad, J. (2016). A complete formulation of an indirect boundary element method for poroelastic rocks. Comput Geotech. 74: 15-25.

[21]. Ghassemi, A., Zhou, X.X. and Rawal, C. (2013). A three-dimensional poroelastic analysis of rock failure around a hydraulic fracture. J Pet Sci Eng. 108: 118-127.

[22]. Huang, J. and Ghassemi, A. (2015). A poroelastic model for evolution of fractured reservoirs during gas production. J Pet Sci Eng. 135: 626-644.

[23]. Safari, R. and Ghassemi, A. (2016). Three-dimensional poroelastic modeling of injection induced permeability enhancement and microseismicity. Int J Rock Mech Min Sci. 84: 47-58.

[24]. Singh, A.K., Yadav, R.P., Kumar, S. and Chattopadhyay, A. (2016). Propagation of crack in a pre-stressed inhomogeneous poroelastic medium influenced by shear wave. Eng Fract Mech. 154: 191-206.

[25]. Remij, E.W., Remmers, J.J.C., Huyghe, J.M. and Smeulders, D.M.J. (2017). An investigation of the step-wise propagation of a mode-II fracture in a poroelastic medium. Mechanics Research Communications. 80: 10-15.

[26]. Abdollahipour, A., Fatehi Marji, M., Yarahmadi Bafghi, A. and Gholamnejad, J. (2016). A complete formulation of an indirect boundary element method for poroelastic rocks. Computers and Geotechnics. 74: 15-25.

[27]. Zhou, Z., Yang, H., Wang, X. and Zhang, Q. (2016). Fractured rock mass hydraulic fracturing under hydrodynamic and hydrostatic pressure joint action. J Cent South Univ. 23: 2695-2704.

[28]. Ren, L., Lin, R., Zhao, J., Yang, K., Hu, Y. and Wang, X. (2015). Simultaneous hydraulic fracturing of ultra-low permeability sandstone reservoirs in China: Mechanism and its field test. J Cent South Univ. 22: 1427-1436.

[29]. Biot, M.A. (1956). General Solutions of the Equations of Elasticity and Consolidation for a Porous Material. ASME J Appl Mech. 78: 91-96.

[30]. Biot, M.A. (1955). Theory of elasticity and consolidation for a porous anisotropic solid. J Appl Phyi. 26: 182-185.

[31]. Biot, M.A. (1941). General theory of three-dimensional consolidation. J Appl Phys.12: 155-164.

[32]. Crouch, S.L. (1983). Starfield AM. Boundary Element Methods in Solid Mechanics. London: George allen & Unwin.

[33]. Fatehi Marji, M. (2015). Higher order displacement discontinuity method in rock fracture mechanics. Yazd University.

[34]. Fatehi Marji, M. (2014). Rock fracture mechanics with displacement discontinuity method. Germany:

LAP Lambert Academic publishing.

[35]. Fatehi Marji, M. (1997). Modelling of cracks in rock fragmentation with a higher order displacement discontinuity method. Middle east technical university.

[36]. Crawford, A.M. and Curran, J.H. (1982). Higher order functional varriation displacement discontinuity elements. Int J Rock Mech Min Sci Geomech Abstr. 19: 143-148.

[37]. Fatehi Marji, M. (2013). On the Use of Power Series Solution Method in the Crack Analysis of Brittle Materials by Indirect Boundary Element Method,. Eng Fract Mech. pp. 365-82.

[38]. Ji, L. (2013). Geomechanical aspects of fracture growth in a poroelastic, chemically reactive environment. The University of Texas at Austin.

[39]. Yin, S., Dusseault, M.B. and Rothenburg, L. (2009). Multiphase poroelastic modeling in semi-space for deformable reservoirs. J Pet Sci Eng. 64: 45-54.

[40]. Yin, S., Dusseault, M.B. and Rothenburg, L. (2007). Analytical and numerical analysis of pressure drawdown in a poroelastic reservoir with complete overburden effect considered. Adv Water Resour. 30: 1160-1167.

[41]. Rice, J.R. and Cleary, M.P. (1976). Some basic stress diffusion solutions for fluid saturated elastic porous media with compressible constituents. Rev Geophys Sp Phys. 14: 227-241.

[42]. Fatt, I. (1958). The Biot-Willis elastic coefficients of a sandstone. J Appl Mech.

[43]. Yew, C. and Jogi, P.N. (1978). The determination of Biot's parameters for sandstones, Part I: static tests. Expl Mech. 18: 167-172.

[44]. Detournay, E. and Cheng, A.H.D. (1993). Fundamentals of Poroelasticity. In: Fairhurst C, editor. Compr. Rock Eng. Princ. Pract. Proj. Vol. II, Anal. Des. Method, Pergamon Press. pp. 113-171.

[45]. Yew, C.H., Jogi, P.N. and Gray, K.E. (1979). Estimation of the mechanical properties of fluid-saturated rocks using the measured wave motions. Journal of Energy Resources Technology. 101 (2): 112-116.

[46]. Erdogan, F. and Sih, G.C. (1963). On the crack extension in plates under plate loading and transverse shear. J Basic Eng. 85: 519-527.

[47]. Sneddon, I.N. (1951). Fourier transforms. New York: McGraw-Hill Book Company.

[48]. Rito, F. and Emura, T. (2013). Sampling method and pore water pressure measurement in the great depth (-400m). Proc. 18th Int. Conf. Soil Mech. Geotech. Eng., Paris. pp. 607-610.

Appendix

Eqs. (A.1)-(A.8) describe the complete stress and displacement fields, pore pressure, and flux in a poroelastic medium [1].

$$(u_{ij})^0 = -\frac{1}{4\pi(1-\nu_u)}\delta(t)\frac{1}{r}\left[(1-2\nu_u)(\delta_{ij}r_{,2}+\delta_{i2}r_{,j}-\delta_{j2}r_{,i})+2r_{,i}r_{,j}r_{,2}\right] \quad \text{(A.1)}$$

$$\begin{aligned}\Delta u_{ij} &= \frac{c(\nu_u-\nu)}{\pi(1-\nu_u)(1-\nu)}\frac{1}{r^3}\Big[2(\delta_{j2}r_{,i}-r_{,i}r_{,j}r_{,2})\xi^4 e^{-\xi^2} \\ &-(\delta_{i2}r_{,j}+\delta_{j2}r_{,i}+\delta_{ij}r_{,2}-4r_{,i}r_{,j}r_{,2})\left(1-e^{-\xi^2}-\xi^2 e^{-\xi^2}\right)\Big]\end{aligned} \quad \text{(A.2)}$$

$$\begin{aligned}(\sigma_{ijk})^0 &= -\frac{G}{2\pi(1-\nu_u)}\delta(t)\frac{1}{r^2}\Big[8r_{,i}r_{,j}r_{,k}r_{,2}-2(\delta_{k2}r_{,i}r_{,j}+\delta_{ij}r_{,k}r_{,2}) \\ &-(\delta_{ik}\delta_{j2}+\delta_{jk}\delta_{i2}-\delta_{ij}\delta_{k2})\Big]\end{aligned} \quad \text{(A.3)}$$

$$\begin{aligned}\Delta\sigma_{ijk} &= -\frac{2Gc(\nu_u-\nu)}{\pi(1-\nu)(1-\nu_u)}\frac{1}{r^4}\Big(\big[24r_{,i}r_{,j}r_{,k}r_{,2}-12(\delta_{ij}r_{,k}r_{,2}+\delta_{k2}r_{,i}r_{,j}) \\ &-3(\delta_{ik}\delta_{j2}+\delta_{jk}\delta_{i2}-3\delta_{ij}\delta_{k2})\big]\left[1-(1+\xi^2)e^{-\xi^2}\right] \\ &-\left[12r_{,i}r_{,j}r_{,k}r_{,2}-6(\delta_{k2}r_{,i}r_{,j}+\delta_{ij}r_{,k}r_{,2})-2\delta_{ik}\delta_{j2}-2\delta_{jk}\delta_{i2}+4\delta_{ij}\delta_{k2}\right]\xi^4 e^{-\xi^2} \\ &-\left[4r_{,i}r_{,j}r_{,k}r_{,2}-4(\delta_{ij}r_{,k}r_{,2}+\delta_{k2}r_{,i}r_{,j})+4\delta_{ij}\delta_{k2}\right]\xi^6 e^{-\xi^2}\Big)\end{aligned} \quad \text{(A.4)}$$

$$(p_i)^0 = \frac{BG(1+\nu_u)}{3\pi(1-\nu_u)}\delta(t)\frac{1}{r^2}(\delta_{i2}-2r_{,i}r_{,2}) \quad \text{(A.5)}$$

$$\Delta p_i = \frac{4BGc(1+\nu_u)}{3\pi(1-\nu_u)}\frac{1}{r^4}\left(\delta_{i2}\xi^4 e^{-\xi^2}+2(r_{,i}r_{,2}-\delta_{i2})\xi^6 e^{-\xi^2}\right) \quad \text{(A.6)}$$

$$(q_{ij})^0 = \frac{3c(\nu_u-\nu)}{\pi B(1-\nu)(1+\nu_u)}\delta(t)\frac{1}{r^3}(\delta_{i2}r_{,j}+\delta_{j2}r_{,i}+\delta_{ij}r_{,2}-4r_{,i}r_{,j}r_{,2}) \quad \text{(A.7)}$$

$$\Delta q_{ij} = -\frac{6c^2(\nu_u-\nu)}{\pi B(1-\nu)(1+\nu_u)}\frac{1}{r^5}\left[2(\delta_{i2}r_{,j}+\delta_{ij}r_{,2}-3\delta_{j2}r_{,i})\xi^6 e^{-\xi^2}+4(\delta_{j2}r_{,i}-r_{,i}r_{,j}r_{,2})\xi^8 e^{-\xi^2}\right] \quad \text{(A.8)}$$

where $(u_{ij})^0$, $(\sigma_{ijk})^0$, $(p_i)^0$, and $(q_{ij})^0$ are the undrained parts showing the time-independent behavior of the material, and Δu_{ij}, $\Delta\sigma_{ijk}$, Δp_i, and Δq_i are drained parts, showing the time-dependent behavior of the materials; u_{ij} is the displacement. It should be noted that the first subscript in u_{ij} presents the displacement component and the second subscript (and the last subscript in any other parameter) denotes the dislocation mode (1 shows the slip mode and 2 shows the normal mode), σ_{ijk} is the stress field, p_i is the pore pressure, and q_{ij} is the flux.

رفتار شکست هیدرولیکی در محیط نفوذپذیر

ابوالفضل عبدالهی پور[۱*]، محمد فاتحی مرجی[۲]، حمید سلطانیان[۱] و عزت ا... کاظم زاده[۱]

۱- پژوهشکده مهندسی نفت، پژوهشگاه صنعت نفت، ایران

۲- دانشکده مهندسی معدن و متالورژی، دانشگاه یزد، ایران

ارسال ۲۰۱۷/۸/۱۶، پذیرش ۲۰۱۸/۶/۹

* نویسنده مسئول مکاتبات: Abdollahipoura@ripi.ir

چکیده:

نفوذپذیری و رفتار توأمان فشار منفذی و تغییر شکل نقش مهمی در مدل‌سازی شکست هیدرولیکی دارند. در این پژوهش، با استفاده از روش ناپیوستگی جابجایی توسعه داده‌شده برای محیط پوروالاستیک اثر نفوذپذیری بر گسترش شکست هیدرولیکی در سازند متخلخل با نفوذپذیری‌های مختلف بررسی شد. مدل عددی استفاده شده توسط حل‌های تحلیلی و نتایج آزمایشگاهی و میدانی موجود اعتبارسنجی شد. سپس گسترش شکست هیدرولیکی در محیط متخلخل با دامنه متفاوتی از نفوذپذیری بررسی شده است. زمان لازم برای گسترش شکست هیدرولیکی به ده برابر طول اولیه آن به عنوان مبنا برای مقایسه سرعت گسترش شکستگی در محیط‌های با نفوذپذیری مختلف استفاده شد. نتایج نشان داد که سرعت گسترش شکست هیدرولیکی در نفوذپذیری‌های کمتر از $۱۰^{-۹}$ دارسی به شدت کاهش می‌یابد. همچنین اثر فاصله‌داری شکستگی بر مسیر رشد شکست هیدرولیکی بررسی شد. نشان داده شد که اثر سایه تنش در محیط پوروالاستیک بیشتر از محیط الاستیک است. در نتیجه پیشنهاد می‌شود در مطالعه گسترش چندگانه شکست هیدرولیکی از مدل پوروالاستیک استفاده شود تا از خطاهای ناشی از نادیده گرفتن اثرات سیال منفذی بر مسیر گسترش شکست هیدرولیکی پرهیز شود.

کلمات کلیدی: شکست هیدرولیکی، محیط پوروالاستیک، نفوذپذیری، گسترش ترک.